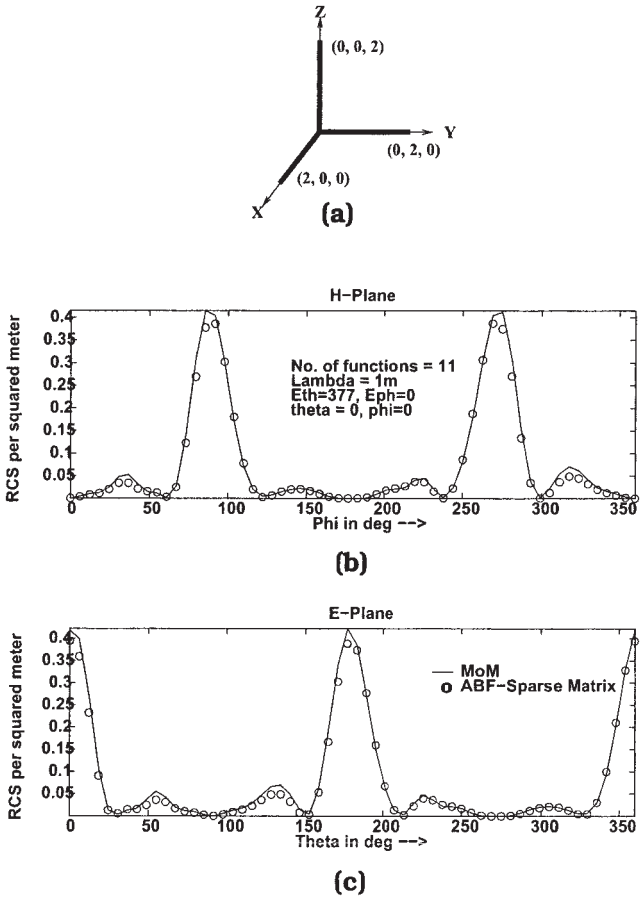

Figure 6 Scattering from the wire structure with geometrically shaped coordinate axes: (a) wire structure; (b) H-plane: $\theta = 90°$ cut; (c) E-plane: $\phi = 0°$ cut

At the outset, we mentioned that the present algorithm has been tested for a variety of wire geometries and in each case the numerical results, that is, the current distribution and RCS compared very well with the standard MoM solution. In Table 1, we present several numerical examples involving a variety of geometrical shapes and incident fields. We note that the parameter K represents the number of nonzero elements in each column for the $N \times N$ matrix. Also, for the illustration purposes, we discuss a few numerical examples as follows.

As a first example, let us consider a 30λ long wire that is bent into the shape of an S, as shown in Figure 2(a). In the numerical solution, the wire is divided into 300 equal-length linear segments, resulting in 299 unknowns. The H-plane and E-plane scattering cross sections for the traditional MoM solution are shown in Fig. 2(b) and 2(c), respectively, along with the ABF banded matrix solution. In order to create the banded impedance matrix, 11 functions are gathered into the cluster. In this plot, there is good agreement between the traditional method and the ABF method.

Next, we consider a sectoral loop, as illustrated in Figure 3(a). The total length of the loop is 32λ. In the numerical solution, we have divided the sectoral wire into 315 linear divisions, giving 315 unknowns. Figures 3(b) and 3(c) compare the H-plane and E-plane patterns, respectively, between the traditional MoM and ABF banded matrix solutions. It may be noted that the two methods match well, as in the previous case.

In the next three examples, we consider wire junctions. The junctions are: (i) T-junction, (ii) Y-junction, and (iii) the three-wire mutually perpendicular junction that resembles the X–Y–Z coordinate axes. The geometry H-plane and E-plane patterns for each case are shown in Figures 4, 5, and 6, respectively. The incident-field parameters are indicated in the inset of the figures. Once again, we note a favorable comparison for each case using the traditional MoM.

5. CONCLUSION

In this work, we have presented a technique to obtain a sparse moment matrix. We used the MoM incorporated with adaptive basis functions for obtaining such a matrix. We have used this technique for a number of wire structures, especially those involving junctions. Junctions are important for modeling 3D surface structures. The results obtained with and without implementing the adaptive basis functions were found to be quite similar.

REFERENCES

1. J.H. Richmond, A wire-grid model for scattering by conducting bodies, IEEE Trans Antennas Propagat AP-14 (1966), 782–786.
2. A.C. Ludwig, Wire grid modeling of surfaces, IEEE Trans Antennas Propagat AP-35 (1987), 1045–1048.
3. R.F. Harrington, Origin and development of the method of moments for field computation in Computational electromagnetics: Frequency-domain method of moments, eds. E.K. Miller, L. Medgyesi-Mitschang, and E.H. Newman, IEEE Press, New York; 1992.
4. D.R. Wilton and C.M. Bulter, Effective methods for solving integral and integro-differential equations, Electromagn 1 (1981), 289–308.
5. E.K. Miller, L. Medgyesi-Mitschang, and E.H. Newman, Computational electromagnetics: Frequency-domain method of moments, IEEE Press, New York, 1992.
6. R.F. Harrington, Field computation by moment methods, Macmillan, New York, 1968.
7. S.M. Rao and M.L. Waller, Development and application of adaptive basis functions to generate diagonal moment matrix for electromagnetic field problems, Microwave Opt Technol Lett 28 (2001), 357–361.
8. S.M. Rao and M.L. Waller, Application of adaptive basis functions for a diagonal moment matrix solution of two dimensional field problems: TE case, Microwave Opt Technol Lett 28 (2001), 270–273.

DISTORTION PRODUCED BY RF MEMS VARACTORS ON DIGITAL COMMUNICATION SIGNALS

Antonio Lázaro,[1] David Girbau,[2] and Lluís Pradell[2]
[1] Department of Electronics, Electrics, and Automatic Engineering
Universitat Rovira i Virgili (URV)
43007, Av. Països Catalans
26, Campus Sescelades
Tarragona, Spain
[2] Department of Signal Theory and Communications
Universitat Politècnica de Catalunya (UPC)
Campus Nord UPC—Mòdul D3
Jordi Girona 1-3
08034 Barcelona, Catalunya, Spain

Received 8 August 2005

ABSTRACT: *This paper presents a study of the nonlinear effects introduced by MEMS varactors when excited with digitally modulated RF signals (QPSK and 16 QAM). The study is based on simulating a nonlinear model of the MEMS device using harmonic-balance and envelope solvers, and on experimental measurements of the wave reflected by the on-wafer MEMS device. It is shown that the adjacent-channel power ratio (ACPR) and error-vector magnitude (EVM) of the digital signal*

suffer a degradation due to the device nonlinear distortion. © 2005 Wiley Periodicals, Inc. Microwave Opt Technol Lett 48: 246–249, 2006; Published online in Wiley InterScience (www.interscience.wiley.com). DOI 10.1002/mop.21318

Key words: *MEMS; RF power handling; adjacent channel power ratio (ACPR); intermodulation distortion*

1. INTRODUCTION

MEMS-based variable capacitors (varactors) have demonstrated a good performance in terms of loss and tuning range, making them suitable for RF applications such as low phase noise VCOs, capacitive switches, phase shifters, tuners, and reconfigurable filters [1, 2]. However, two phenomena arise, namely, power handling [3] and intermodulation distortion (IMD) [1, 5], that limit full integration of MEMS devices in power transmitters. These unwanted effects are produced by the device nonlinear behaviour, not only in MEMS varactors, but also in RF MEMS switches. Concerning the IMD issue, an analytical method is proposed in [1], giving expressions to predict two-tone IMD products in MEMS capacitive switches. However, the behaviour of MEMS varactors excited with digitally modulated communication signals (QPSK, QAM, . . .) has not been yet studied. It is known that two-tone IMD tests cannot generally predict nonlinear effects associated with digital modulations, such as the adjacent-channel power ratio (ACPR). The purpose of this paper is to study the effect of the MEMS varactors' nonlinearity on digital communication systems. The study is based on computer simulations and experimental work in which digitally modulated RF signals are injected into the MEMS varactor. Two effects are observed, namely, the ACPR degrades while the bit error rate (BER) and error-vector magnitude (EVM) increase. The MEMS device was modelled as in [1, 4], and the simulations are performed on it using the circuit solvers (harmonic balance and envelope mode) included in the Agilent ADS simulator™ without any simplifications or linearisation of the device model. In this way, high-order intermodulation products can be considered. This is advantageous with respect to the method proposed in [5], where expressions for 5th or higher orders are possible using Volterra series, but limited to weak nonlinearities. Simulations and on-wafer measurements at 1.2 GHz of the reflected waves in a MEMS varactor (PolyMUMPS™ process), excited by QPSK and 16-QAM signals, are presented for different transmission velocities and RF input powers.

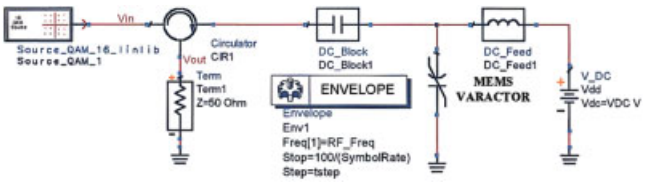

Figure 2 Schematic used for envelope harmonic simulation of the varactor model implemented using Agilent ADS. [Color figure can be viewed in the online issue, which is available at www.interscience.wiley.com.]

2. MEMS CAPACITOR MODEL, SIMULATION, AND EXPERIMENTAL SETUPS

Consider a MEMS device based on a suspended mobile membrane, excited by a signal composed of two RF tones at nearby frequencies f_1 and f_2. If $|f_2 - f_1| < f_{res}$ and $f_{1,2} \gg f_{res}$, where f_{res} is the mechanical resonance frequency of the membrane, then the membrane gap is modulated at a frequency $|f_2 - f_1|$ due to the quadratic dependence of the force on the applied voltage. In [1], it was shown that such a modulation in MEMS capacitive switches produces IMD products in the output RF voltage at frequencies $|2f_1 - f_2|$ and $|2f_2 - f_1|$. This effect can also be seen as a modulation of the device reflection coefficient phase at a frequency $|f_2 - f_1|$, which in turn produces the abovementioned IMD products in the reflected RF voltage. Measurement of the reflected wave is preferred in MEMS varactors, where the reflection coefficient magnitude is high [6]. If the device is excited with a digitally modulated RF signal (which can be wideband), the phase modulation effects are noticed as a degradation of ACPR, BER and EVM. Figure 1 shows the proposed experimental setup, which includes a directional coupler to extract the reflected wave, vector signal generator with power amplifier and circulator, wafer-probe station, and spectrum analyzer. To study those effects theoretically, a nonlinear simulation is implemented using the envelope harmonic simulation mode supported by ADS. To model the MEMS varactor, the 1D dynamic equation for equivalent mass-spring-damping model for electrostatically actuated MEMS [1] is used.

Figure 2 shows the ADS schematic proposed. An input digitally modulated signal is injected to the MEMS varactor and, by using an ideal circulator, the reflected voltage wave in the nonlinear capacitance is obtained. It is similar to the experimental setup of Figure 1, but the reflectometer is implemented with an ideal circulator.

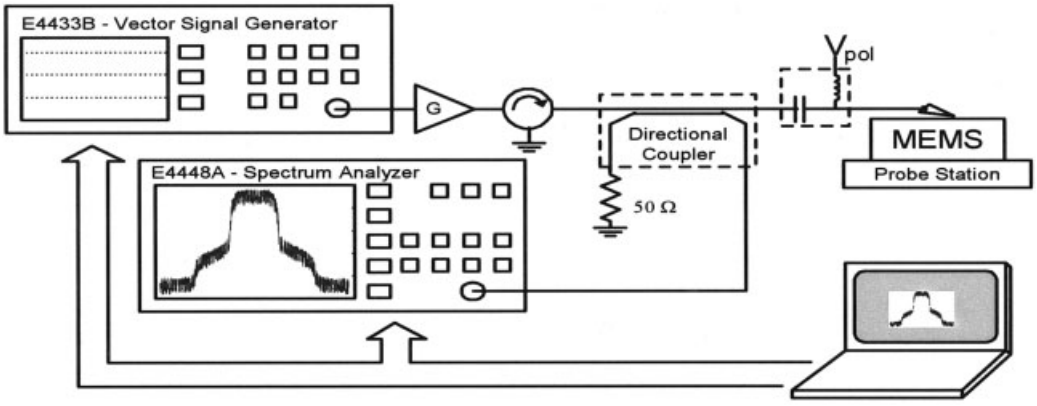

Figure 1 Experimental setup

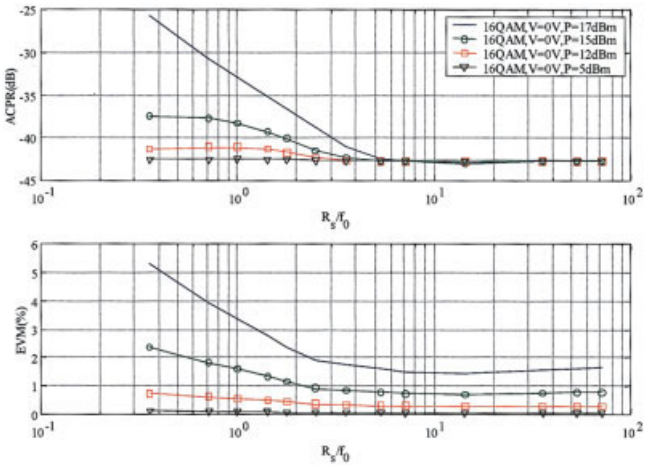

Figure 3 Simulated ACPR (dBc) and EVM (%) of varactor for a 16-QAM signal with several input RF powers: ▼ $P = 5$ dBm; □ $P = 12$ dBm; ○ $P = 15$ dBm; – $P = 17$ dBm. [Color figure can be viewed in the online issue, which is available at www.interscience.wiley.com.]

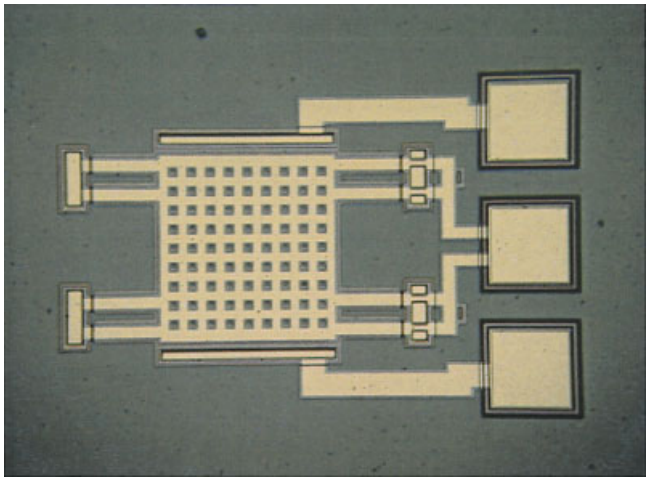

Figure 5 Measured MEMS variable capacitor. [Color figure can be viewed in the online issue, which is available at www.interscience.wiley.com.]

To study the nonlinear effects of a MEMS varactor on digital modulations, we use the model shown in Figure 2 to perform simulations of ACPR and EVM produced by the MEMS varactor (see Fig. 5 below). The simulated device is a two parallel-plate varactor manufactured using PolyMUMPs™ process. The effective parameters of the device are: spring constant $k = 35$ N/m, mechanical quality factor $Q = 0.3$, natural resonant frequency $f_0 = 14$ kHz, initial gap distance $g_0 = 0.75$ μm, nominal capacity 1.43 pF, parasitic capacity $C_p = 2.58$ pF, electrical quality factor $Q_e = 13$ at 1.2 GHz, and pull-in voltage $V_p = 2$. As a consequence of this low pull-in voltage, we expect poor nonlinear behaviour to be exhibited.

Figure 3 shows the results of the simulated ACPR and EVM in the reflected wave for a 16-QAM modulated signal as a function of the symbol rate (normalized to the mechanical resonant frequency f_0). ACPR and EVM worsen for signals with a symbol rate lower than the mechanical resonant frequency. This effect increases with increasing RF signal power, because the mean gap decreases with the RF voltage (self-actuation), thus enhancing the effects of nonlinearity. For symbol rates much higher than the mechanical resonant frequency, the ACPR level improves but the EVM remains almost constant because the varactor can only produce slow phase variations in the external symbols of the constellation. Figure 4 shows simulated ACPR and EVM in the reflected wave, for a 16-QAM modulated signal as a function of the applied DC bias voltage, normalized to the device pull-in voltage V_p. The ACPR degrades and EVM increases for increasing bias, due to a lower position of the membrane.

The measurements are performed at 1.2 GHz, using the experimental setup of Figure 1. Figure 6 shows the reflected power spectrum, measured at the reflectometer output for two input powers (10 and 17 dBm) when 16 QAM is injected with a symbol rate of 10 KHz (root-cosine filter with a rollof factor of 0.3). The measured ACPR strongly increases with increasing RF power. The measured mechanical resonance frequency using the system proposed in [6] is about 14 kHz. Figure 7 shows the measured and simulated ACPR produced by this device as a function of symbol rate for 16-QAM and QPSK signals with high power level (17 dBm). The ACPR rapidly improves for symbol rates higher than the mechanical resonance, thus verifying the tendency shown in

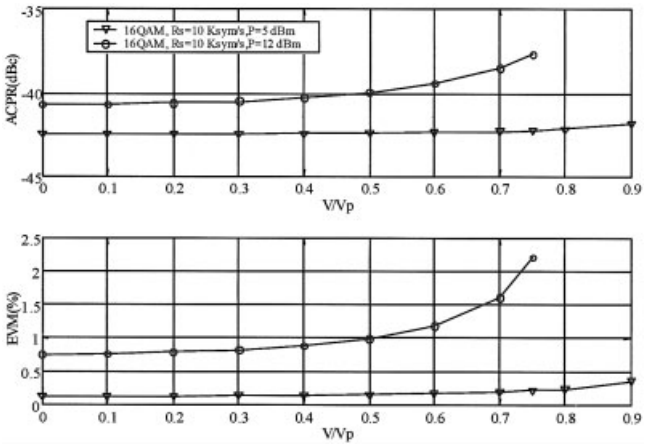

Figure 4 Simulated ACPR (dBc) and EVM (%) for 16-QAM, Rs = 10 Ksym/s as a function of normalized applied DC bias (V/Vp): ▼ $P = 5$ dBm; ○ $P = 12$ dBm

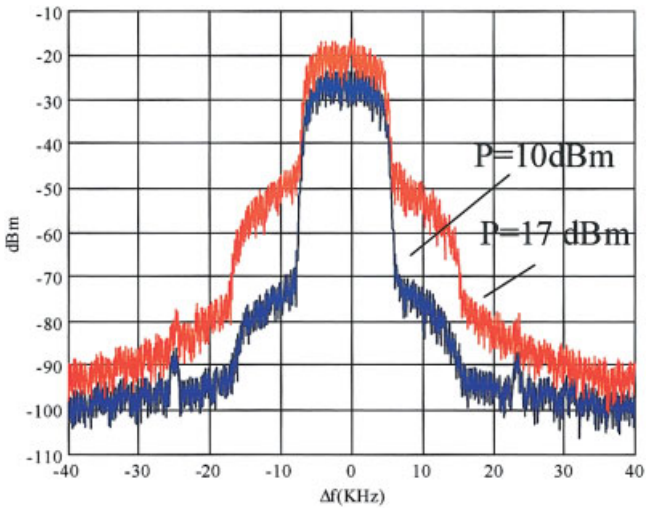

Figure 6 Measured reflected output power spectrum at 1.2 GHz for 16-QAM signal (filter rollof factor = 0.3). [Color figure can be viewed in the online issue, which is available at www.interscience.wiley.com.]

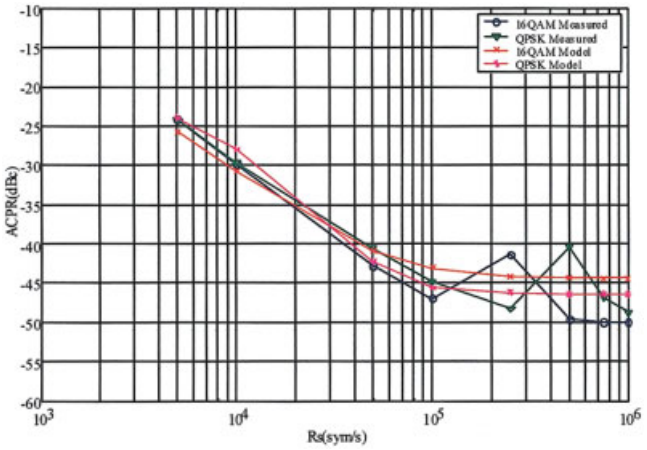

Figure 7 Measured and simulated ACPR (dBc) for digitally modulated QPSK (▼) and 16 QAM (○) signals as a function of symbol rate R_s (RF input power is 17 dBm). [Color figure can be viewed in the online issue, which is available at www.interscience.wiley.com.]

the simulations. Figure 8 shows the measured ACPR for 16-QAM and QPSK signals as a function of the input power for two symbol rates: 10 KHz ($<f_0$) and 100 KHz ($\gg f_0$). The ACPR degrades with increasing RF signal input power, being higher for lower symbol rates in both modulations.

Figure 9 shows the simulated ACPR for the MEMS capacitor, as a function of input power and pull-in voltage (or spring constant). Good agreement between the simulated and measured results is obtained. This figure also shows a rapid increase of the ACPR level with the input RF power. The ACPR rapidly degrades when the input power is close to the power handling.

3. CONCLUSION

In this paper, the effects of the nonlinearity of MEMS-based varactors on digitally modulated signals have been investigated by performing envelope harmonic-balance simulations on a 1D electromechanical model and by measuring the device using the proposed experimental setup. Important effects such as, in particular, a degradation in ACPR and an increase in EVM, have been observed (in the simulations and measurements) for digitally modulated signals with low-to-moderate symbol rate and high power. This effect is quite important for low pull-in voltage structures, generally designed for voltage levels compatible with standard CMOS ICs. Therefore, a limit is imposed upon the RF power that communication systems using these varactors can handle. From the results, it is advisable to work with high-symbol-rate signals, as they produce lower IMD in MEMS-based circuits.

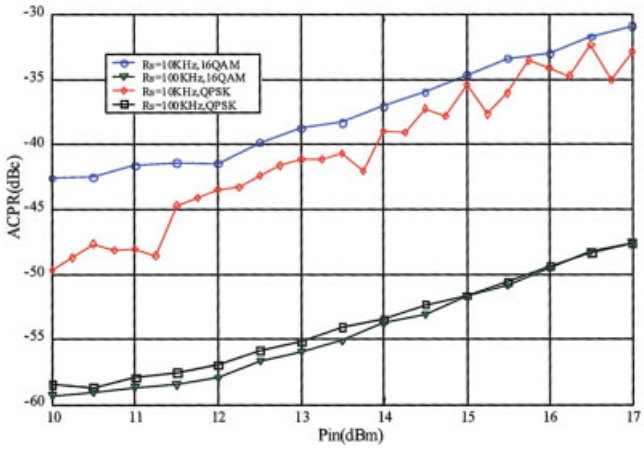

Figure 8 Measured ACPR (dBc) vs. input power for: ○ 16QAM/R_s = 10 KHz; ▼ 16 QAM/R_s = 100 KHz; ◇ QPSK/R_s = 10 KHz; □ QPSK/R_s = 100 KHz. [Color figure can be viewed in the online issue, which is available at www.interscience.wiley.com.]

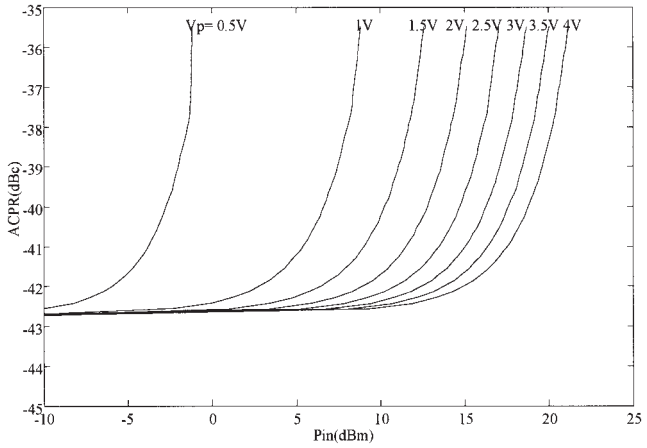

Figure 9 Simulated ACPR (dBc) vs. input power (dBm) for several pull-in voltages (modulation: 16 QAM, symbol rate R_s = 10 KHz)

ACKNOWLEDGMENT

This work was supported by the Spanish Government under grant nos. TIC2000-0144-P4-02 and ESP2004-07067-C03-03 (MCYT).

REFERENCES

1. L. Dussopt and G.M. Rebeiz, Intermodulation distortion and power handling in RF MEMS switches, varactors and tunable filters, IEEE Trans Microwave Theory Tech 51 (2003), 1247–1256.
2. A. Dec and K. Suyana, Microwave MEMS-based voltage-controlled oscillators, IEEE Trans Microwave Theory Tech 48 (2000), 1943–1949.
3. D. Peroulis, S.P. Pacheco, and L. Katehi, RF MEMS switches with enhanced power-handling capabilities, IEEE Trans Microwave Theory Tech 52 (2004), 59–68.
4. D. Mercier, P. Blondy, et al., Model for MEMS switches power handling and phase noise, 32nd Eur Microwave Conf, Milan, Italy, 2002, pp. 219–222.
5. M. Innocent, P. Wambacq, S. Donnay, H.A.C. Tilmans, W. Sansen, and H. De Man, An analytic Volterra-series-based model for a MEMS variable capacitor, IEEE Trans computer-aided design Integrated Circ Syst 22 (2003), 124–131.
6. D. Girbau, A. Lázaro, and L. Pardell, Characterization of dynamics and power handling of RF MEMS using vector measurement techniques, IEEE Trans Microwave Theory Tech 52 (2004), 2627–2633.